Reduction-Triggered Self-Cross-Linked Hyperbranched Polyglycerol Nanogels for Intracellular Delivery of Drugs and Proteins

Haeree Park, Yeongkyu Choi, M. T. Jeena, Eungjin Ahn, Yuri Choi, Myeong-Gyun Kang, Chae Gyu Lee, Tae-Hyuk Kwon, Hyun-Woo Rhee, Ja-Hyoung Ryu, and Byeong-Su Kim*

Owing to the unique advantages of combining the characteristics of hydrogels and nanoparticles, nanogels are actively investigated as a promising platform for advanced biomedical applications. In this work, a self-cross-linked hyperbranched polyglycerol nanogel is synthesized using the thiol–disulfide exchange reaction based on a novel disulfide-containing polymer. A series of structural analyses confirm the tunable size and cross-linking density depending on the type of polymer (homo- or copolymer) and the amount of reducing agent, dithiothreitol, used in the preparation of the nanogels. The nanogels retain not only small molecular therapeutics irrespective of hydrophilic and hydrophobic nature but also large enzymes such as β-galactosidase by exploiting the self-cross-linking chemistry. Their superior biocompatibility together with the controllable release of active therapeutic agents suggests the applicability of nanogels in smart drug delivery systems.

1. Introduction

Nanogels are aqueous dispersions of hydrogel particles in the nanometer range, which are formed from physically or chemically cross-linked polymeric networks.[1–3] Owing to the unique advantages that combine the characteristics of hydrogels and nanoparticles, nanogels are actively investigated as promising platforms for advanced biomedical applications.[4–8] In contrast to other self-assembled nanostructures, nanogels are more stable and have longer circulation times. Specifically, the

development of nanogels in drug delivery could address a range of challenges to allow precise control over properties such as structure, size, surface functionality, hydrophilic/hydrophobic balance, and drug loading capacity.[9–12] When responsive polymers are exploited as building blocks for nanogels, smart nanogels can be prepared that stably encapsulate therapeutic molecules and release them in response to specific stimuli such as pH,[13–15] temperature,[16,17] redox,[18–22] light,[23,24] and enzyme activity.[25,26]

Nanogels are generally prepared by microemulsion or inverse microemulsion methods. However, these conventional methods are relatively complex and require multiple purification steps to remove unreacted monomers and the surfactants used as emulsion stabilizers. Moreover, these methods have drawbacks, such as limited types of internal payload. On the other hand, the formation of nanogels from linear polymers by intra- and interchain collapse can afford a facile protocol toward well-defined delivery vehicles. This method also often requires very dilute conditions and thus potentially limits encapsulation efficiency.

Hyperbranched polyglycerols (PGs) are among the most widely used hyperbranched polymers, and possess a globular polymeric structure comprised of a polyether backbone with a large number of hydroxyl groups. PGs are actively investigated as an alternative to conventional poly(ethylene glycol), the most biocompatible synthetic polymer, in broad applications such as surfactants, cosmetics, and pharmaceutics owing to their excellent biocompatibility, immunogenicity, and oxidation stability.[27–30] Moreover, recent advances in the development of functional epoxide monomers have expanded the toolkit for the synthesis of functional hyperbranched PGs with responsive properties under specific biological cues. For example, a glycerol monomer containing a disulfide bond, that is, 2-((2-(oxiran-2-ylmethoxy) ethyl)disulfanyl) ethan-1-ol (SSG), was recently developed by our group to synthesize redox-degradable hyperbranched PGs (PSSGs).[31,32] These PSSGs can offer new opportunities in smart drug delivery systems by taking advantage of considerable redox concentration gradients between intracellular and extracellular environments. Even with these developments, the loading of active therapeutics for redox-responsive

H. Park
Department of Chemical Engineering
Ulsan National Institute of Science and Technology (UNIST)
Ulsan 44919, Korea

Dr. Y. Choi, M. T. Jeena, Y. Choi, M.-G. Kang, C. G. Lee, Prof. T.-H. Kwon, Prof. H.-W. Rhee, Prof. J.-H. Ryu, Prof. B.-S. Kim
Department of Chemistry
Ulsan National Institute of Science and Technology (UNIST)
Ulsan 44919, Korea
E-mail: bskim19@unist.ac.kr

E. Ahn, Prof. B.-S. Kim
Department of Energy Engineering
Ulsan National Institute of Science and Technology (UNIST)
Ulsan 44919, Korea

The ORCID identification number(s) for the author(s) of this article can be found under https://doi.org/10.1002/mabi.201700356.

ADVANCED
SCIENCE NEWS
www.advancedsciencenews.com

Macromolecular
Bioscience
www.mbs-journal.de

PSSGs was limited because of the intrinsic hydrophilicity of hyperbranched PSSGs.

Thus, in continuation of our endeavors in the development of hyperbranched PGs for biomedical applications, we herein demonstrate the synthesis of redox-responsive nanogels from hyperbranched PSSGs that can encapsulate a variety of internal payloads such as hydrophobic/hydrophilic drugs and enzymes. Specifically, we exploited the self-cross-linking chemistry of thiol and disulfide groups within polymeric structures after the addition of a deficient amount of dithiothreitol (DTT) (**Figure 1**). By varying many synthetic parameters including the fraction of degradable monomers within the polymers (homo- and copolymers), molecular weights, and the degradation degree according to equivalents of a disulfide cleavage agent, we tailored the size and mesh density of the nanogels, which in turn controlled the release profiles of their internal payloads. The nanogel formation employed in the present study circumvents the aforementioned synthetic challenges, generating water-soluble nanogels with high encapsulation capabilities of various active therapeutics and biocompatibility while retaining the responsive behavior for smart drug delivery.
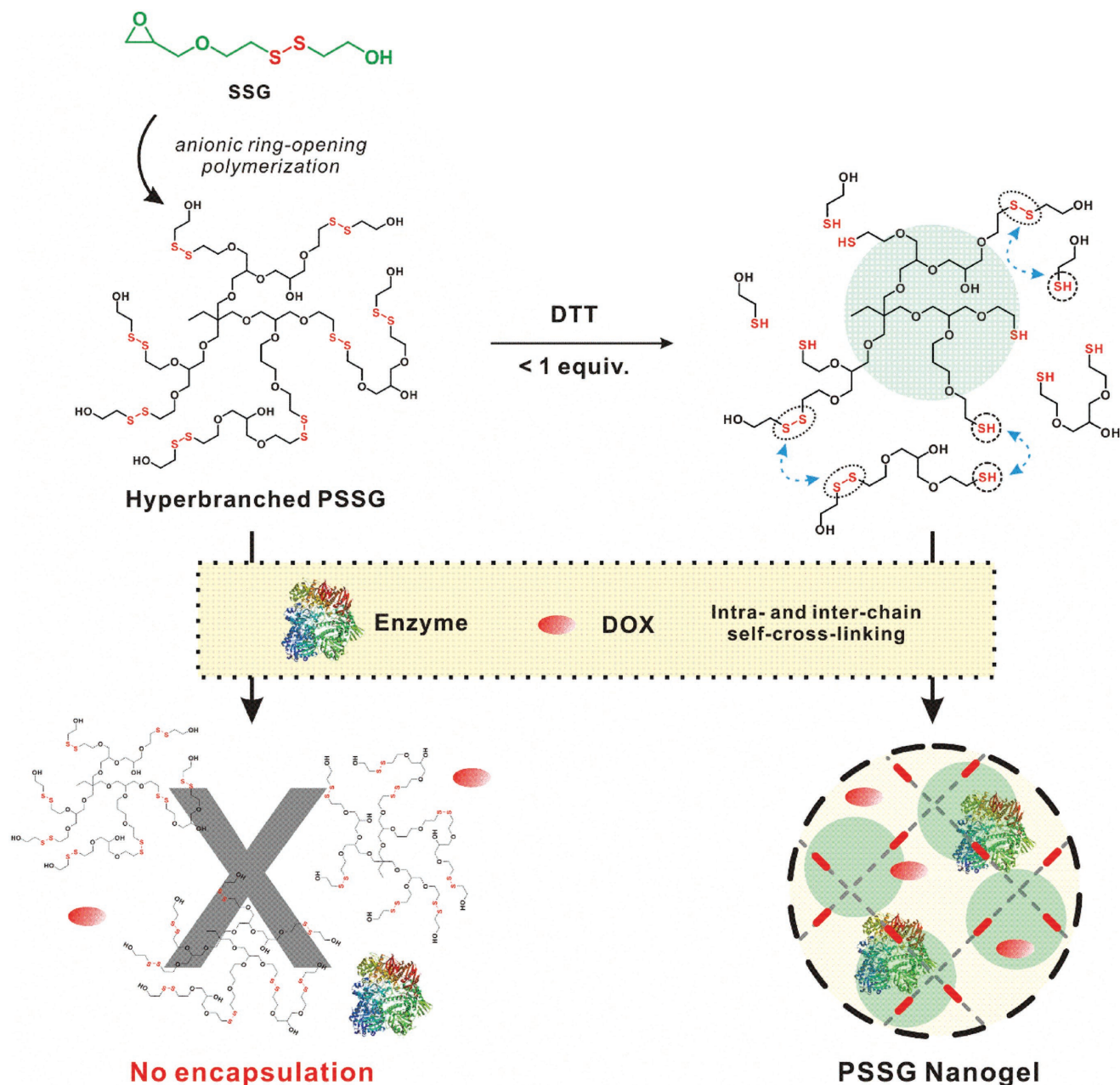
Figure 1. Synthetic scheme for the PSSG polymer and the in situ formation of degradable nanogels through thiol–disulfide exchange and disulfide exchange chemistry (marked with blue arrows) between inter- and intramolecular chains upon treatment with DTT. Other chains are not depicted for clarity. Green circle represents the basic unit for the formation of the PSSG nanogel.

2. Experimental Section

2.1. Materials

All reagents and solvents were purchased from Sigma-Aldrich and Acros and used as received unless otherwise stated. Chloroform-d_1 and deuterium oxide were purchased from Cambridge Isotope Laboratory. Doxorubicin hydrochloride (Dox·HCl) was purchased from EP (France). The X-gal assay kit was purchased from BioVision, Inc., USA.

2.2. Synthesis of 2-((2-(Oxiran-2-ylmethoxy) ethyl)disulfanyl) ethan-1-ol (SSG Monomer), (PSSG Homopolymer), and (P(G-co-SSG) Copolymer)

The SSG monomer and polymer were prepared according to the previous report (see Figures S1 and S2, Supporting Information, for details).[31]

2.3. In Situ Formation of Redox-Sensitive Nanogels

50 mg of P(G_{10}-co-SSG_{12}) polymer (polymer 3) was dissolved in 1.0 mL deionized water and placed in a flask preheated at 70 °C for 10 min. A predetermined amount of DTT (0.2 and 1.0 mg) that corresponded to 10 and 50 mol% of DTT relative to the disulfide moieties, respectively, was added to the polymer solution and stirred at room temperature for 15 h to allow for degradation and subsequent inter- and intramolecular cross-linking. The resulting nanogels were purified by dialysis (MWCO 6000 Da, SpectraPore, USA) for 3 d to eliminate any by-products and residual DTT. After purification, the concentration of nanogel was determined to be 5.5 mg mL^{-1} by gravimetric analysis (11% isolated yield).

2.4. Nanogels Encapsulated with Hydrophobic Nile Red

50 mg of P(G_{10}-co-SSG_{12}) polymer (polymer 3) and excess Nile red (2 mg) were dissolved in 200 µL of acetone and a measured amount of DTT (0, 0.2, and 1.0 mg, which corresponded to 0, 10, and 50 mol% of DTT relative to the disulfide moieties) was added. After stirring for 10 min, 1.0 mL of deionized water was added, and the mixture was stirred overnight at room temperature while open to the atmosphere, allowing the organic solvent to evaporate. Insoluble excess Nile red aggregates were removed by filtration (PTFE Syringe Filter, 0.45 µm), and the nanogel suspension was dialyzed as described above.

2.5. Release of Encapsulated Nile Red from Nanogel

A 1.0 mL sample of nanogel with encapsulated Nile red was placed inside a dialysis membrane (MWCO 500–1000 Da, SpectraPore, USA) for 72 h. The fluorescence intensity of the nanogel in the dialysis membrane was determined using a spectrofluorometer at an excitation wavelength of 480 nm and emission wavelength of 638 nm with a constant time interval during the release of Nile red through dialysis membrane against deionized water. In active release case, a 1.0 mL sample of nanogel with encapsulated Nile red was placed inside a dialysis membrane (MWCO 500–1000 Da, SpectraPore, USA) under reductive condition (10 equiv. against nanogel) for 72 h.

2.6. Nanogel Encapsulated with Dox

50 mg of P(G_{10}-co-SSG_{12}) polymer (polymer 3) was dissolved in 5.0 mL of deionized water and DTT (0, 0.2, and 1.0 mg, which corresponded to 0, 10, and 50 mol% of DTT relative to the polymers, respectively) was added to the solution. Afterward, Dox from Dox·HCl (7.5 mg, 0.013 mmol) pretreated with 50% NaOH solution was added slowly into the solution. The pH was adjusted to 7.4 with a phosphate buffer solution (solution mixture of 10×10^{-3} M KH_2PO_4 and K_2HPO_4). The mixture was stirred for 24 h at room temperature and dialyzed against PBS buffer (pH 7.4) using a dialysis membrane (MWCO 6000 Da, SpectraPore, USA) for 3 d at room temperature while water was changed every day.

2.7. In Vitro Cell Cytotoxicity

The cytotoxicity and efficacy of the nanogels in drug delivery were assessed by thiazolyl blue tetrazolium bromide (MTT) assays. Briefly, HeLa cells (human epithelial carcinoma cells) and WI-38 cell (human diploid cells) purchased from the Korea Cell Line Bank (Korea) grew in 96-well plate containing Dulbecco's modified Eagle's medium (DMEM), 10% fatal bovine serum (FBS), and 1% penicillin-streptomycin at a density of 3×10^4 cells per well. After stabilizing, the HeLa and WI-38 cells were treated with each nanogel solution and incubated for 24 h at 37 °C in a humidified atmosphere of 95% air/5% CO_2. MTT (Sigma-Aldrich) was added in each well (final conc. of 0.50 mg mL^{-1}) and incubated for 3 h. After removing the culture medium, 100 µL of DMSO was added to each cell well to dissolve the MTT reagent, and the plates were gently agitated for 15 min at room temperature. The absorbance was measured at a wavelength of 540 nm using 620 nm as a reference.

2.8. Cellular Uptake of Nanogels

Cellular uptake of Dox-loaded nanogels and pure nanogels was measured with confocal laser fluorescence microscopy imaging using HeLa cells. HeLa cells were plated on microscope slides in an eight-well tissue culture plate at a density of 3×10^4 cells per well and incubated with DMEM containing 10% FBS and 1% penicillin-streptomycin for 24 h. After preincubating, the Dox-loaded nanogels were dissolved in the culture medium to a concentration of 0.50 mg mL^{-1} for an additional 6 and 24 h. After washing with PBS (pH 7.4), a solution of 4′,6-diamidino-2-phenylindole (DAPI, Sigma-Aldrich; 20 mg mL^{-1} in MEM media) was incubated at 37 °C. The cells were fixed with 4% formaldehyde at room temperature after 30 min incubation. Confocal laser scanning microscopy (CLSM) images were taken using a Carl Zeiss LSM880 confocal microscope.

ADVANCED
SCIENCE NEWS
www.advancedsciencenews.com

Macromolecular
Bioscience
www.mbs-journal.de

2.9. Preparation of Fluorescein Isothiocyanate Isomer I-Labeled β-Galactosidase (FITC-β-gal) and Dox-Loaded Nanogels

50 mg of P(G$_{10}$-co-SSG$_{12}$) polymer (polymer 3) was dissolved in 1.0 mL of deionized water and DTT (1.0 mg, which corresponded to 50 mol% of DTT relative to the disulfide moieties, respectively) was added in the solution. Afterward, Dox (2 mg, 3.7 µmol) and FITC-β-gal (conc. 0.20 mg mL^{-1}) were added slowly into the solution. FITC labeling of the β-galactosidase was performed according to the previously reported procedure.[41] The mixture was kept stirring for 24 h at room temperature and dialyzed against PBS buffer using a dialysis membrane (MWCO 6000 Da, SpectraPore, USA) for 3 d at room temperature while water was changed every day. The obtained product was centrifuged to separate the unencapsulated free β-gal for 10 min at 4000 rpm.

2.10. Confocal Analysis of FITC-Labeled β-Galactosidase-Loaded Nanogels

The cellular internalization of FITC-labeled β-gal-loaded nanogels and intracellular release were monitored with confocal microscopic analysis. The HeLa cells were seeded in eight-well tissue culture plates at a density of 3×10^3 cells per well. After 24 h, the culture medium was exchanged with fresh medium and further treated with nanogels loaded with both Dox and FITC-β-gal at a concentration of 1.0 mg mL^{-1} for 6 h at 37 °C under 5% CO$_2$. CLSM images were taken using an Olympus LSM-780 confocal microscope.

2.11. Activity Assay of β-Galactosidase Loaded in Nanogels (X-gal Staining)

HeLa cells were seeded in a 12-well tissue culturing plate at 5×10^4 cells/well supplemented with DMEM medium containing 10% FBS and 1% penicillin-streptomycin. After 24 h, the culture medium was removed and exchanged with fresh media containing both Dox and FITC-β-gal-loaded nanogel 4 at a concentration of 1.0 mg mL^{-1}. After 24 h, the cells were washed with PBS and X-gal staining was carried out according to the manufacturer's instructions (BioVision, USA). Briefly, cells were fixed with the fixative for 15 min followed by washing with PBS twice, then supplemented with staining materials (470 µL of staining solution, 5 µL of staining supplement, 25 µL of 20 mg mL^{-1} of X-gal in DMF), and kept overnight at 37 °C in a non-CO$_2$ incubator. After 12 h, cells were washed with PBS and imaged with an OLYMPUS inverted fluorescence microscope.

2.12. Measurements

^{1}H NMR spectra were acquired using a VNMRS 600 spectrometer operating at 400 MHz using D$_2$O solvents. The number (M_n) and weight-averaged molecular weights (M_w) and molecular-weight distribution (M_w/M_n) were measured using gel permeation chromatography (GPC, Agilent Technologies 1200 series, USA) with a polystyrene (PS) standard and 0.01 M lithium bromide containing dimethylformamide (DMF) as an eluent at 40 °C with a flow rate of 1.00 mL min^{-1}. The morphology and the size of the nanogels were investigated using transmission electron microscopy (TEM, JEM-2100, JEOL, Japan) and atomic force microscopy (AFM, Dimension 3100, Veeco, USA). Hydrodynamic diameter (D_h) was studied using dynamic light scattering (DLS, Nano ZS, Malvern, UK, and BI-APD, Brookhaven Instrument, New York, USA). Three instruments were used to cross-check the reliability of the obtained data. A UV–vis spectrophotometer (UV-2550, Shimadzu, Japan) was used to measure the absorbance of nanogels containing Nile red. A spectrofluorimeter (RF-6000, Shimadzu, Japan) was also used to obtain the release profiles of dyes from nanogels and to determine the amount of encapsulated FITC-β-gal within nanogels. The calibration curve of doxorubicin (Dox) was obtained by high-performance liquid chromatography (HPLC, Agilent Technologies 1200 series, USA) with a mobile phase of a mixture of CH$_3$CN and H$_2$O (6:4, v/v) at a rate of 0.80 mL min^{-1} and 20 °C. The detection of Dox was performed by using a UV detector at a wavelength of 480 nm. The fluorescent images were obtained by CLSM (LSM880, LSM 780, Carl Zeiss, Germany). The X-gal activity assay was carried out with an OLYMPUS Inverted Fluorescence Microscope.

3. Results and Discussion

3.1. Synthesis and Characterizations of Polymer and Nanogel

To provide redox-degradable hyperbranched polyglycerols, we first prepared the SSG monomer as reported previously.[31,32] After synthesis of the SSG monomer, we performed the polymerization to PSSG homopolymers and P(G-co-SSG) copolymers via anionic ring-opening multibranching polymerization methods. Five different hyperbranched polymers (both homo- and copolymers) of varying molecular weights ranging from 2240 to 10 890 g mol^{-1} were successfully prepared, as determined by ^{1}H NMR and GPC analyses (**Table 1**). We found relatively good agreement between the targeted and calculated molecular weights of polymers that were controlled by the monomer-to-initiator ratio, albeit with noticeable differences in their respective reactivities during polymerization (see the Experimental Section for detailed calculations and Figure S2, Supporting Information, for ^{1}H NMR spectra). GPC analysis also allowed the characterization of the controlled polymerization of homopolymers and copolymers in a relatively narrow molecular weight distribution ($M_w/M_n < 1.5$).

Unlike other studies that described treatment with excess DTT to cleave all redox-degradable moieties, we hypothesized that the addition of an insufficient amount of DTT would cause the cleavage of a well-defined fraction of disulfide groups from the corresponding thiol functionalities. These thiol functionalities would then react with other free thiols either in the same polymer or in neighboring chains to form new disulfide bonds or with other existing disulfide groups in thiol–disulfide exchange chemistry. It is well known that these reactions occur reversibly at room temperature in water without the need for additional catalysts and chemicals.[33] Thus, a series of these reactions eventually results in cross-links within the polymeric aggregates, leading to the formation of nanogels, as shown in Figure 1. As notable examples, Thayumanavan and co-workers

ADVANCED
SCIENCE NEWS
www.advancedsciencenews.com

Macromolecular
Bioscience
www.mbs-journal.de

Table 1. Characterization data of polymers used in this study.

Entry	Polymer composition (target)	Polymer composition (NMR)[a]	M_n (target)	% SSG (target)	M_n (NMR)[a]	% SSG (NMR)[a]	M_n (GPC)[b]	M_w/M_n (GPC)[b]
1	PSSG$_{10}$	PSSG$_{11}$	2240	100	2450	100	3600	1.53
2	PSSG$_{30}$	PSSG$_{30}$	6440	100	6440	100	6300	1.30
3	P(G$_{10}$-co-SSG$_{20}$)	P(G$_{10}$-co-SSG$_{12}$)	5080	66.7	3400	54.6	4400	1.24
4	P(G$_{20}$-co-SSG$_{20}$)	P(G$_{21}$-co-SSG$_{13}$)	5820	50.0	4420	38.2	5000	1.25
5	P(G$_{60}$-co-SSG$_{30}$)	P(G$_{46}$-co-SSG$_{18}$)	10890	33.3	7460	28.1	5400	1.38

[a]Determined via ^{1}H NMR spectroscopy; [b]Measured using GPC-RI in DMF with a polystyrene standard.

have employed the self-cross-linking chemistry of disulfide groups for the formation of various types of nanogels.[10,11,34,35]

3.2. Size Controllable Nanogels with Varying Amount of DTT

To investigate the effect on the formation of nanogels with different amounts of DTT, we prepared nanogels treated with 10–50 mol% of DTT relative to the polymer (**Figure 2**a). In this

study, we choose DTT instead of biological reducing agent, glutathione (GSH), as the reducing performance and stability of DTT is higher than GSH as reported in the previous report. As representative examples, we chose homopolymer PSSG$_{30}$ (polymer 2) and copolymer P(G$_{10}$-co-SSG$_{12}$) (polymer 3) for the formation of nanogels.

As clearly observed in the AFM images of the nanogels in Figure 2b, both polymers successfully formed nanogels after treatment with defined amounts of DTT. Interestingly, the
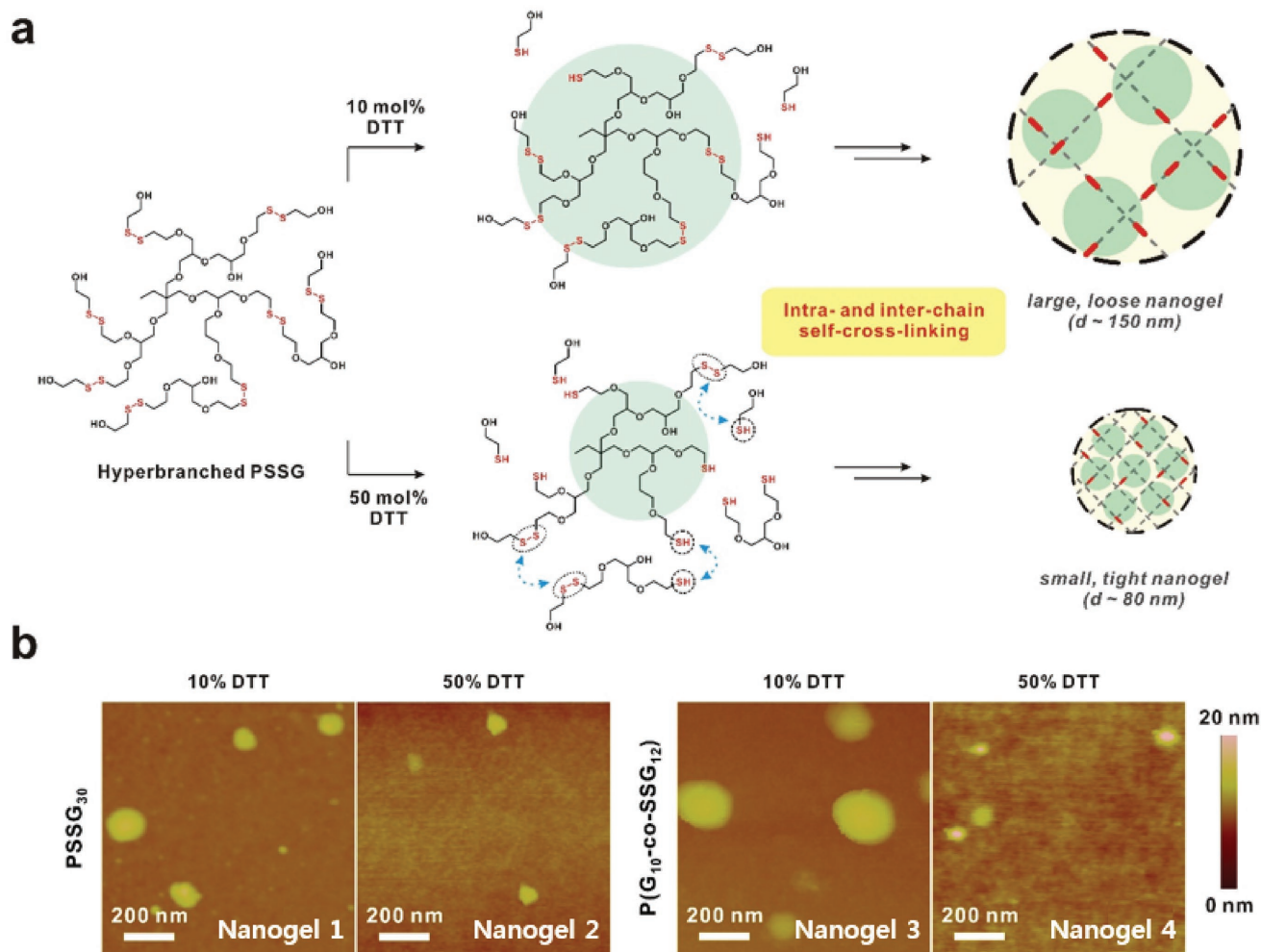
Figure 2. a) Scheme for the synthesis of size-controllable PSSG nanogels with different amounts of DTT. b) Representative AFM images of nanogels prepared from PSSG$_{30}$ homopolymer (polymer 2) and P(G$_{10}$-co-SSG$_{12}$) copolymer (polymer 3) with 10 and 50 mol% of DTT.

ADVANCED
SCIENCE NEWS
www.advancedsciencenews.com

Macromolecular
Bioscience
www.mbs-journal.de

Table 2. Characterization data of nanogels prepared in this study.

Nanogel	Polymer[a]	DTT [mol%]	AFM [nm]	TEM [nm]	DLS [nm]
Nanogel 1	$PSSG_{30}$	10	142 ± 30	194 ± 34	220 ± 52
Nanogel 2	$PSSG_{30}$	50	78 ± 8.3	57 ± 6.7	85 ± 14
Nanogel 3	$P(G_{10}\text{-}co\text{-}SSG_{12})$	10	178 ± 54	168 ± 42	249 ± 71
Nanogel 4	$P(G_{10}\text{-}co\text{-}SSG_{12})$	50	74 ± 12	80 ± 16	79 ± 21

[a]Concentration of all polymers is 50 mg mL^{-1}.

controlled sizes of cross-linked nanogels were shown with average diameters of 142 ± 30 and 78 ± 8.3 nm for nanogels prepared from $PSSG_{30}$ homopolymer, and 178 ± 54 and 74 ± 12 nm for $P(G_{10}\text{-}co\text{-}SSG_{12})$ copolymer with 10 and 50 mol% DTT treatment, respectively (**Table 2**). This observation can be explained on the basis of the balance between the degradation of the polymer into smaller fragments and subsequent reassembly into cross-linked nanogels. Specifically, it suggests that the nanogels prepared by treatment with a smaller amount of DTT (i.e., 10 mol%) were less cross-linked because smaller quantities of free thiols were allowed to react with disulfide groups or thiol groups in other chains, eventually leading to large, yet loosely cross-linked nanogels. TEM images further supported that these nanogels possessed a spherical morphology with a particle size in accordance with the AFM results (Figure S3, Supporting Information).

In parallel, DLS studies indicated that the hydrodynamic diameters (D_h) of nanogels obtained from $P(G_{10}\text{-}co\text{-}SSG_{12})$ copolymers treated with various concentrations of DTT were significantly changed from the pristine polymers (**Figure 3**). For example, the D_h of nanogels prepared by treatment with 10, 20, and 50 mol% DTT were 249 ± 71, 203 ± 52, and 79 ± 21 nm, respectively. Interestingly, the D_h of pristine $P(G_{10}\text{-}co\text{-}SSG_{12})$ copolymer itself indicated a D_h of only 2 nm, clearly demonstrating the absence of self-aggregation of the initial polymers without the introduction of reducing
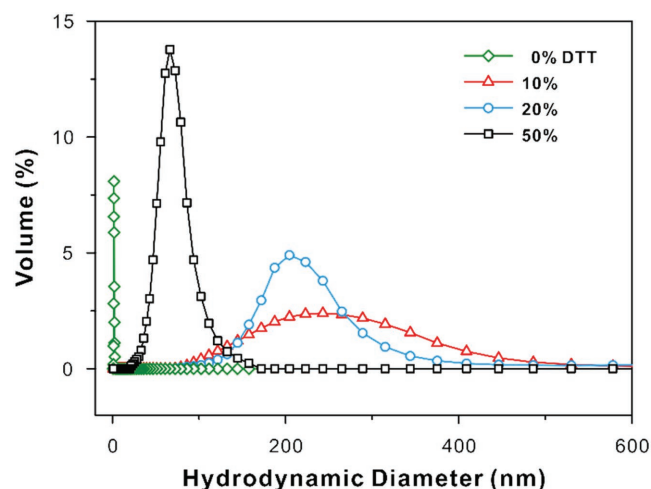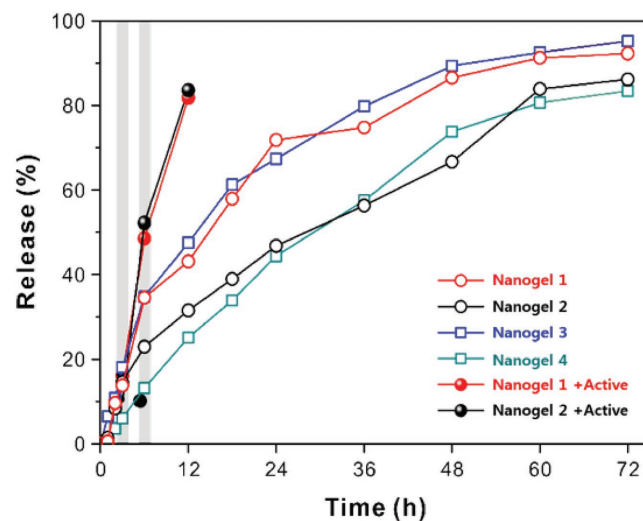
chemicals. The average D_h values (obtained using DLS) of the nanogels were slightly larger than those observed by AFM and TEM, which can be attributed to the swelling of the nanogels in water (Table 2). We also monitored the size tunability of nanogels upon changes in the concentration of the initial polymer solution; for example, when the concentration was doubled to 100 mg mL^{-1}, the D_h of nanogel 4 increased considerably from 79 ± 21 to 585 ± 102 nm. We attributed this size increase to the enhanced probability of polymeric segment to reassemble into larger-sized nanogels.

3.3. Release Kinetics of Therapeutics from Nanogels

To investigate the stability of the nanogels, we characterized the encapsulation efficiency using the hydrophobic Nile red stain as a model therapeutic payload. Because of the limited aqueous solubility of Nile red, we used acetone as a cosolvent during the formation of the nanogels and simultaneous loading of Nile red. The relative encapsulation efficiency of Nile red is considerably different between the nanogels. For example, nanogel 2 retained a significantly higher loading of ≈8 times than that of nanogel 1, albeit with smaller dimensions, as determined by AFM and DLS. The loading capacity for each nanogel 1 and nanogel 2 was determined to be 0.68 and 0.81% (wt of Nile red/wt of nanogel), respectively. Similarly, nanogel 4 displayed a 12 times higher loading capacity of Nile red per unit volume than nanogel 3. Thus, loading capacity depends on cross-linking density. This result again highlights the high tunability of our nanogels in terms of loading capacity with the facile treatment of a reducing chemical reagent.

Furthermore, we investigated the release of Nile red encapsulated within nanogels. As shown in **Figure 4**, large and loosely cross-linked nanogel 1 and nanogel 3 both demonstrated more rapid release, while small and densely cross-linked nanogel 2 and nanogel 4 displayed a slower release over time. This observation may suggest that the cross-linking density is

Figure 3. Hydrodynamic diameter (D_h) of nanogels prepared from $P(G_{10}\text{-}co\text{-}SSG_{12})$ copolymer (polymer 3) with varying degrees of DTT treatment. Note that the D_h of the initial $P(G_{10}\text{-}co\text{-}SSG_{12})$ copolymer (green) is determined to be only 2 nm.

Figure 4. Release profile of Nile red from nanogels with different cross-linking densities. Note that the shaded time points represent treatment of the Nile red-loaded nanogels with additional DTT for an active delivery mode.

responsible for controlling the rate of payload release from the nanogels.

Another interesting feature of the redox-responsive nanogel system is that it can further release the internal payload in response to additional reducing stimuli. Because the nanogels are still cross-linked by disulfide bonds, Nile red can be further released upon treatment with DTT as an active delivery mode. It should be noted here that unlike the nanogel formation which required a lower equivalence of reducing chemical, here, we used excess of DTT to completely degrade all the reducible bonds present within the nanogel. As such, when we introduced additional DTT at a designated time point, we could observe the enhanced release kinetics. For example, the relative release percentages of Nile red from nanogel 1 and nanogel 2 for 12 h are 43 and 32%, respectively, in the case of passive release. On the other hand, the relative release percentages from nanogel 1 and nanogel 2 are 82 and 84%, respectively, in the active release mode. Consequently, the addition of DTT (10 equiv. against nanogel) to stable nanogels containing active therapeutic agents can facilitate more rapid release than that of the nanogels alone. Taken together, we argue that redox-degradable nanogels can be beneficial in achieving active therapeutic delivery with a wide range of tunability in their size and controllable release kinetics, which can potentially be applied in response to the higher reducing environments inside the cytoplasm.

3.4. In Vitro Cell Viability and CLSM Images

Encouraged by the successful synthesis and control over the release kinetics of the model therapeutic from the nanogels, we evaluated their cytotoxicity to investigate their potential in biomedical settings. The in vitro cytotoxicity of each nanogel was assessed via the MTT assay using WI-38 and HeLa cell lines as models of normal and cancer cells, respectively (Figure S5, Supporting Information). The cell viability of each cell line treated with the polymeric nanogels was greater than 80%, even up to a concentration of 1000 µg mL^{-1}, which is beyond the common concentration ranges usually tested. These results indicate that

all nanogels are highly biocompatible (<1000 µg mL^{-1}) and nontoxic to both cell lines.

Moreover, in vitro efficacy for the intracellular delivery of the active therapeutic agent from Dox-loaded nanogels was investigated by a cell viability assay using a human cervical cancer HeLa cell line. As shown in **Figure 5**a, the Dox-loaded nanogel 4 nanogels induced significant cytotoxicity in HeLa cells, while virtually no toxicity was observed from nanogel 4 over the entire concentration range tested (see Figure S6, Supporting Information, for all nanogels tested). The concentration at which the cell viability decreased to 50% using Dox/nanogel 4 was estimated to be ≈0.04 × 10^{-6} M of Dox as determined from HPLC. This value is found to be higher than the reported IC$_{50}$ of Dox (≈0.015 × 10^{-6} M).[36]

The cellular uptake efficiency of Dox-loaded nanogel 4 was further studied by CLSM (Figure 5b). The encapsulated Dox was slowly released when the Dox-loaded nanogel 4 was delivered at the cell cytoplasm, which spread to all parts of the cytoplasm within 6 h. After 24 h, it was found inside the nucleus and several pores were generated by cellular apoptosis induced by the effective delivery of Dox. It was observed that the Dox-loaded nanogel 4 was located within the endosomal vesicles, releasing Dox in a controlled manner.

3.5. Codelivery Efficacy of the Drug-Loaded Nanogels In Vitro

Combination therapies are of special interest and provide a high potential for increased efficacy through synergistic interplay between therapeutics.[37–40] Simultaneous delivery of proteins and small molecular drugs is a compelling strategy that has been employed in cancer therapy and immunotherapy.[41] One key challenge in the codelivery of active therapeutic agents is the distinct physicochemical properties required for each component, particularly for hydrophobic and hydrophilic components, such as in the delivery of hydrophobic small molecules along with large hydrophilic proteins.

We hypothesize in this study that concurrent delivery of enzyme and active drug is indeed feasible with
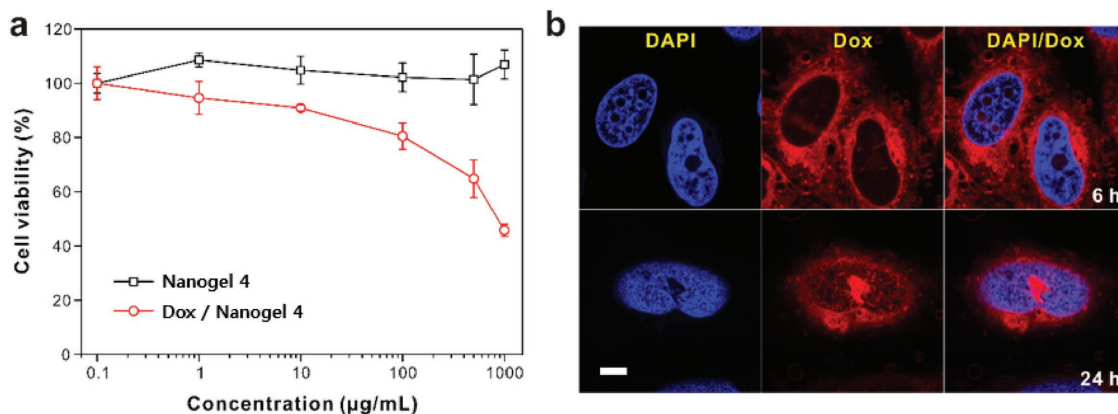
Figure 5. a) In vitro cell viability assay of plain nanogel 4 (black) and Dox-loaded nanogel 4 (red). b) CLSM images of HeLa cells incubated with Dox-loaded nanogel 4 for 6 h (top panel) and 24 h (bottom panel). Each channel corresponds to the fluorescence of DAPI for cell nucleus and Dox for drug delivery. Scale bar is 20 µm.
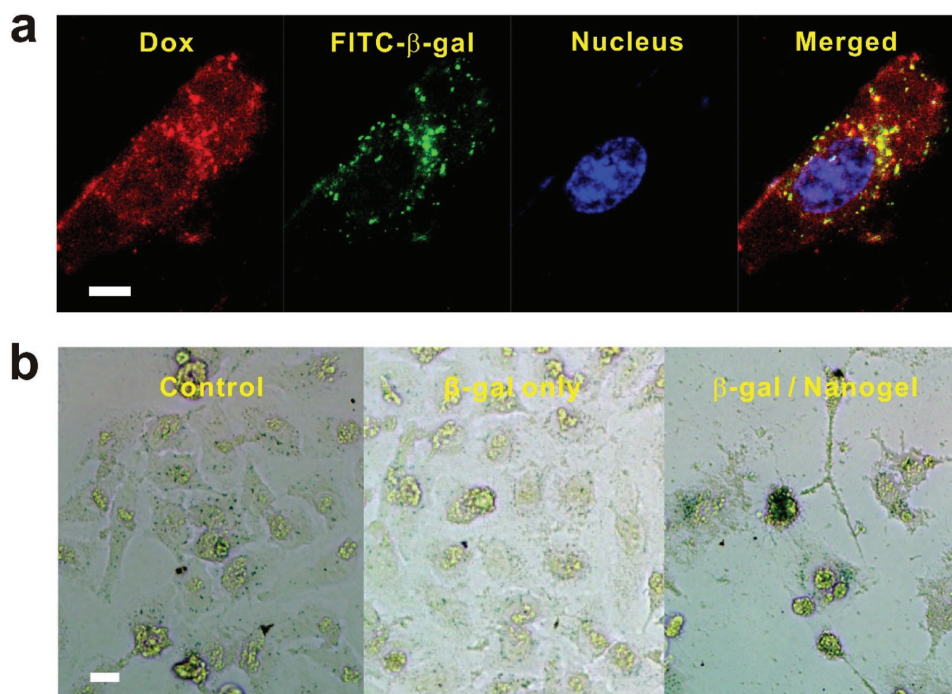
Figure 6. a) CLSM images of HeLa cells incubated with nanogel 4 loaded with both Dox and the FITC-labeled β-galactosidase (FITC-β-gal). Each channel corresponds to the red color of Dox, the green for FITC-β-gal, and the blue Hoechst stain in the cell nucleus. b) X-gal activity assay of delivered β-gal into HeLa cells using nanogel 4. Control samples of free cells and β-gal only. Note that the free cells indicate the X-gal activity due to the presence of internal β-gal in the lysosome. Scale bar is 10 µm.

redox-responsive nanogels. As a proof-of-concept, we employed the β-galactosidase functionalized with fluorescein (FITC-β-gal) as a hydrophilic protein and Dox as a hydrophobic small therapeutic encapsulated within the nanogel 4 (see the Experimental Section for details). When the nanogel 4 dual-loaded with Dox and FITC-β-gal was incubated with HeLa cells for 12 h, Dox was transported into the cytosol and nucleus, while FITC-β-gal existed in the lysosome as shown in **Figure 6**a. As the nanogels consist of bioreducible disulfide bonds, the release of the encapsulated protein and small molecule can be triggered upon exposure to GSH, a biological cue present at higher concentration inside cells than in the extracellular environment. The colocalization of both Dox and FITC-β-gal was successfully confirmed by the overlay of each fluorescence color in the merged image, suggesting the effective intracellular delivery of nanogels regardless of the size and types of payload. Based on the fluorescence intensity measurement, the amount of loaded FITC-β-gal was determined to be about 8.6 µg mL^{-1} at a concentration of 50 mg mL^{-1} of nanogel 4. In addition, the D_h of nanogel 4 loaded with both FITC-β-gal and Dox is larger than pure nanogel 4 and nanogel 4 loaded with only FITC-β-gal (Figure S7, Supporting Information).

Finally, we demonstrated that the protein activity is retained after internalization into the cells using the X-gal activity assay (Figure 6b). The HeLa cells incubated with nanogel 4 loaded with β-gal exhibited a dark blue color because of the conversion of the 5-bromo-3-indoyl-β-D-galactopyranoside into a corresponding indigo derivative by β-gal. In contrast, the control experiment revealed a weak blue color scattered inside the cells because of the presence of internal β-gal in the lysosome. Moreover, considering that the cellular membrane is not permeable to β-gal itself and that the hydrophobic dye is not soluble in water, these results confirmed the critical role of nanogels in the concurrent delivery of a functional protein and a therapeutic agent inside the cells.

4. Conclusions

In summary, we developed a self-cross-linked hyperbranched polyglycerol nanogel using the thiol–disulfide exchange reaction based on a novel disulfide-containing polymer. The highly tunable nature of the size and cross-linking density of the resulting nanogel was controlled by the type of polymer (homo- or copolymer) and the amount of reducing agent, dithiothreitol, used in the preparation of the nanogels. In situ encapsulation of various therapeutic agents irrespective of hydrophilic and hydrophobic nature and molecular weight was accomplished with the intra- and intermolecular thiol–disulfide exchange reaction and new disulfide bond formation within hyperbranched polymers. Their superior biocompatibility together with the controllable release of active therapeutic agents that are still functional inside cells show the applicability of nanogels in smart drug delivery systems. We anticipate that redox-responsive nanogels will provide a promising platform to mediate the delivery of a wide range of active therapeutics in a time-specific and stimulus-specific manner.

Supporting Information

Acknowledgements

Conflict of Interest

The authors declare no conflict of interest.

Keywords

[1] R. T. Chacko, J. Ventura, J. Zhuang, S. Thayumanavan, *Adv. Drug Delivery Rev.* **2012**, *64*, 836.

[2] X. Zhang, S. Malhotra, M. Molina, R. Haag, *Chem. Soc. Rev.* **2015**, *44*, 1948.

[3] H. Q. Wu, C. C. Wang, *Langmuir* **2016**, *32*, 6211.

[4] J. K. Oh, R. Drumright, D. J. Siegwart, K. Matyjaszewski, *Prog. Polym. Sci.* **2008**, *33*, 448.

[5] A. L. Sisson, R. Haag, *Soft Matter* **2010**, *6*, 4968.

[6] Z. An, Q. Qiu, G. Liu, *Chem. Commun.* **2011**, *47*, 12424.

[7] E. Fleige, M. A. Quadir, R. Haag, *Adv. Drug Delivery Rev.* **2012**, *64*, 866.

[8] S. Y. An, D. Arunbabu, S. M. Noh, Y. K. Song, J. K. Oh, *Chem. Commun.* **2015**, *51*, 13058.

[9] B. D. Steinhilber, A. L. Sisson, D. Mangoldt, P. Welker, K. Licha, R. Haag, *Adv. Funct. Mater.* **2010**, *20*, 4133.

[10] J. H. Ryu, S. Jiwpanich, R. Chacko, S. Bickerton, S. Thayumanavan, *J. Am. Chem. Soc.* **2010**, *132*, 8246.

[11] J. H. Ryu, S. Bickerton, J. Zhuang, S. Thayumanavan, *Biomacromolecules* **2012**, *13*, 1515.

[12] Z. Cao, X. Zhou, G. Wang, *ACS Appl. Mater. Interfaces* **2016**, *8*, 28888.

[13] N. Morimoto, S. Hirano, H. Takahashi, S. Loethen, D. H. Thompson, K. Akiyoshi, *Biomacromolecules* **2013**, *14*, 56.

[14] M. R. Molla, T. Marcinko, P. Prasad, D. Deming, S. C. Garman, S. Thayumanavan, *Biomacromolecules* **2014**, *15*, 4046.

[15] B. Liu, S. Thayumanavan, *J. Am. Chem. Soc.* **2017**, *139*, 2306.

[16] H. J. Moon, D. Y. Ko, M. H. Park, J. M. Kyung, B. M. Jeong, *Chem. Soc. Rev.* **2012**, *41*, 4860.

[17] J. Sun, Z. Yu, C. Hong, C. Pan, *Macromol. Rapid Commun.* **2012**, *33*, 811.

[18] J. Liu, Y. Pang, W. Huang, Z. Zhu, X. Zhu, Y. Zhou, D. Yan, *Biomacromolecules* **2011**, *12*, 2407.

[19] W. Chen, M. Zheng, F. Meng, R. Cheng, C. Deng, J. Feijen, Z. Zhong, *Biomacromolecules* **2013**, *14*, 1214.

[20] H. Urakami, J. Hentschel, K. Seetho, H. Zeng, K. Chawla, Z. Guan, *Biomacromolecules* **2013**, *14*, 3682.

[21] S. Singh, F. Topuz, K. Hahn, K. Albrecht, J. Groll, *Angew. Chem., Int. Ed.* **2013**, *52*, 3000.

[22] N. Chan, S. Y. An, J. K. Oh, *Polym. Chem.* **2014**, *5*, 1637.

[23] T. Nishimura, M. Takara, S. Mukai, S. Sawada, Y. Sasaki, K. Akiyoshi, *Chem. Commun.* **2015**, *52*, 1222.

[24] S. Panja, G. Dey, R. Bharti, P. Mandal, M. Mandal, S. Chattopadhyay, *Chem. Mater.* **2016**, *28*, 8598.

[25] C. Wu, C. Böttcherb, R. Haag, *Soft Matter* **2015**, *11*, 972.

[26] C. Wu, C. Strehmel, K. Achazi, L. Chiappisi, J. Dernedde, M. C. Lensen, M. Gradzielski, M. B. Ansorge-schumacher, R. Haag, *Biomacromolecules* **2014**, *15*, 3881.

[27] A. L. Sisson, D. Steinhilber, T. Rossow, P. Welker, K. Licha, R. Haag, *Angew. Chem., Int. Ed.* **2009**, *48*, 7540.

[28] D. Wilms, S. Stiriba, H. Frey, *Acc. Chem. Res.* **2010**, *43*, 129.

[29] R. A. Shenoi, B. F. L. Lai, M. Imran Ul-Haq, D. E. Brooks, J. N. Kizhakkedathu, *Biomaterials* **2013**, *34*, 6068.

[30] J. Herzberger, K. Niederer, H. Pohlit, J. Seiwert, M. Worm, F. R. Wurm, H. Frey, *Chem. Rev.* **2016**, *116*, 2170.

[31] S. Son, E. Shin, B. S. Kim, *Macromolecules* **2015**, *48*, 600.

[32] S. Son, H. Park, E. Shin, Y. Shibasaki, B. S. Kim, *J. Polym. Sci., Part A: Polym. Chem.* **2016**, *54*, 1752.

[33] R. Singh, G. M. Whitesides, *Sulfur-Containing Functional Groups* (Ed: S. Patai), Wiley, New York **1993**.

[34] J. H. Ryu, R. Roy, J. Ventura, S. Thayumanavan, *Langmuir* **2010**, *26*, 7086.

[35] J. H. Ryu, R. T. Chacko, S. Jiwpanich, S. Bickerton, R. P. Babu, S. Thayumanavan, *J. Am. Chem. Soc.* **2010**, *132*, 17227.

[36] Y. P. Istomin, E. A. Zhavrid, E. N. Alexandrova, O. P. Sergeyeva, S. V. Petrovich, *Exp. Oncol.* **2008**, *30*, 56.

[37] L. Wei, C. Cai, J. Lin, T. Chen, *Biomaterials* **2009**, *30*, 2606.

[38] K. Numata, S. Yamazaki, N. Naga, *Biomacromolecules* **2012**, *13*, 1383.

[39] Y. Kim, C. Kim, S. Song, *ACS Macro Lett.* **2016**, *5*, 297.

[40] M. R. A. Alex, C. Nehate, S. Veeranarayanan, D. S. Kumar, R. Kulshreshtha, V. Koul, *Biomaterials* **2017**, *133*, 94.

[41] D. C. Gonza, J. H. Ryu, R. T. Chacko, J. Zhuang, S. Thayumanavan, *J. Am. Chem. Soc.* **2012**, *134*, 6964.